Trigonal Prismatic Coordination of Discrete Rare Earth Ions, Enforced by the Polyoxotungstate $[P_4W_{27}O_{99}(H_2O)]^{16-}$

Tuba Iftikhar,[a, b] Natalya V. Izarova,*[a, b] Jan van Leusen,[a] and Paul Kögerler*[a, b]

Abstract: A family of solution-stable polyanions $[Na\subset\{Ln^{III}(H_2O)\}\{W^{VI}O(H_2O)\}P^{V}_4W^{VI}_{26}O_{98}]^{12-}$ (Ln = Sm, Eu, Gd, Tb, Dy, Ho, Er, Tm, Yb, Lu and Y) represent the first examples of polyoxometalates comprising a single lanthanide(III) or yttrium(III) ion in a rare trigonal prismatic O_6 environment. Their synthesis exploits the reactivity of the organophosphonate-functionalized precursor $[P_4W_{24}O_{92}(C_6H_5P^{V}O)_2]^{16-}$ with heterometal ions and yields hydrated potassium or mixed lithium/potassium salts of composition $K_xLn_yH_{12-x-y}[Na\subset\{Ln(H_2O)\}\{WO(H_2O)\}P_4W_{26}O_{98}]\cdot nH_2O\cdot m$LiCl ($x = 8.5–11$; $y = 0–2$; $n = 24–34$; $m = 0–1.5$). The Dy, Ho, Er and Yb derivatives are characterized by slow magnetization relaxation.

Introduction

Lanthanide-containing polyoxometalates (POMs, discrete metal oxo clusters) exhibit potential in the areas of catalysis, molecular magnetism, photophysics, and materials science.[1] In such species, the POM frameworks act as rigid, all-inorganic metalloligands that efficiently stabilize either multinuclear lanthanide oxo/hydroxo cores or a specific coordination geometry for a single lanthanide ion. In particular, they can induce highly unusual coordination environments for the heterometal.[2]

Lanthanide-containing POMs (Ln-POMs) were reported already in 1914 with the discovery of $(NH_4)_2[H_6CeMo_{12}O_{42}]\cdot nH_2O$ by Barbieri,[3] yet it took until 1971 when Peacock and Weakley discovered that lacunary polyoxotungstates (POTs) and -molybdates, comprising vacant reactive sites due to removal of one or several M^{VI} constituents (M = Mo, W) from the parent polyanions as a result of carefully controlled hydrolysis processes, act as polydentate O-donor ligands towards rare earth metal ions and were able to isolate $[Ln(W_5O_{18})_2]^{Z-}$ (Ln=La^{III}, Pr^{III}, Nd^{III}, Sm^{III}, Eu^{III}, Ho^{III}, Er^{III}, Yb^{III}, Y^{III}, $Z = 9$; Ln=Ce^{IV}, $Z = 8$) as well as some $[Ln(\alpha\text{-}XW_{11}O_{39})_2]^{Z-}$ (X=P^{V}, Si^{IV}) and $[Ln(\alpha_2\text{-}P_2W_{17}O_{61}]^{Z-}$ derivatives.[4]

Since then, the field of Ln-POMs has expanded enormously, and they now can be classified into three main subclasses: (*a*) polyanions comprising a single Ln^{III} center; (*b*) species incorporating several segregated Ln^{III} ions and (*c*) polyanions integrating a polynuclear oxo/hydroxo cluster of lanthanide ions or both lanthanide and transition metal ions stabilized by lacunary POMs as auxiliary ligands. Representative examples include (*a*) $[Yb^{III}As_2W_{20}O_{68}(H_2O)_3]^{7-}$,[5] $[Ln^{III}(H_2O)P_5W_{30}O_{110}]^{14-}$,[2,6] $[Ln^{III}(\alpha_2\text{-}P_2W_{17}O_{61})_2]^{17-}$;[4,7] (*b*) $[\{(H_2O)_nLn^{III}(\alpha_2\text{-}P_2W_{17}O_{61})\}_2]^{7-}$,[8] $[Ln^{III}{}_8As_4W_{38}O_{132}(H_2O)_{22}(2\text{-picolinate})_8]^{12-}$ (Ln = Tb, Eu),[9] $[Ce^{III}{}_{16}As^{III}{}_{12}W_{148}O_{524}(H_2O)_{36}]^{76-}$,[10] $[Ce^{III}{}_{20}Ge_{10}W_{100}O_{376}(OH)_4(H_2O)_{30}]^{56-}$;[11] (*c*) $[\{Yb^{III}{}_6(\mu_6\text{-}O)(\mu_3\text{-}OH)_6(H_2O)_6\}(P_2W_{15}O_{56})_2]^{14-}$,[12] $[Ce^{IV}{}_7Ce^{III}{}_3O_6(OH)_6(CO_3)(H_2O)_{11}(P_2W_{16}O_{59})_3]^{19-}$,[13] $[Ln^{III}{}_{27}Ge_{10}W_{106}O_{406}(OH)_4(H_2O)_{24}]^{59-}$ (Ln=La, Ce)[14] and $[\{M^{II}(piperazine)_2\}_2\{Ln^{III}{}_{29}Ge_{10}W_{106}O_{406}\text{-}(OH)_4(H_2O)_{28}\}]^{49-}$ (M=Cu, Co, Ni; Ln=La, Ce).[14]

Due to the high magnetic moments combined with pronounced magnetic anisotropy of Ln^{III} ions, caused by strong spin-orbit coupling, numerous Ln-POMs exhibit single-molecule magnet characteristics with high effective magnetization relaxation barriers.[15] $[Er^{III}(W_5O_{18})_2]^{9-}$ was among the first examples of single-ion magnets (SIMs).[16] In recent years, several other Ln-containing polyoxotungstate[6b,17] and -molybdate[18] SIMs as well as several Ln-POMs with polynuclear Ln cores[19] exhibiting SMM behavior were reported. Furthermore, the rigidity of the POM matrices, allowing for a control of the electronic structure of the Ln^{III} ions, in conjunction with an ability of nanoscale polyanionic ligands to efficiently isolate a Ln^{III} ion from intermolecular magnetic interactions renders Ln-POMs suitable candidates for quantum computing.[20] $[Gd^{III}(H_2O)P_5W_{30}O_{110}]^{12-}$ polyanions diluted in crystals of the isostructural Y^{III} derivative may act as three-qubit processors implemented within a single Gd^{III} ion.[21] In these species the Gd^{III} center adopts an unusual O_{10} coordination environment of idealized C_{5v} symmetry as well as an apical aqua ligand. For $[Ho^{III}(W_5O_{18})_2]^{9-}$, comprising Ho^{III} ions in a distorted square-antiprismatic coordination environment, quantum coherence could be significantly enhanced via atomic clock transitions, which translated into considerable

[a] T. Iftikhar, Dr. N. V. Izarova, Dr. J. van Leusen, Prof. Dr. P. Kögerler
Institute of Inorganic Chemistry
RWTH Aachen University
D-52074 Aachen (Germany)
E-mail: paul.koegerler@ac.rwth-aachen.de

[b] T. Iftikhar, Dr. N. V. Izarova, Prof. Dr. P. Kögerler
Jülich-Aachen Research Alliance (JARA-FIT) and
Peter Grünberg Institute 6
Forschungszentrum Jülich
D-52425 Jülich (Germany)
E-mail: n.izarova@fz-juelich.de

Supporting information for this article is available on the WWW under https://doi.org/10.1002/chem.202101474

coherence times even without drastic spin dilutions.[22] The potential of cuboid-shaped polyoxopalladate(II) clusters $[LnPd_{12}O_8(PhAsO_3)_8]^{5-}$ incorporating Ln^{III} ions in a cubic O_8 environment as spin qubits was also discussed.[23]

We here report a series of novel $[Na\subset\{Ln^{III}(H_2O)\}\{WO(H_2O)\}P_4W_{26}O_{98}]^{12-}$ (Ln = Sm (**Sm1**), Eu (**Eu2**), Gd (**Gd3**), Tb (**Tb4**), Dy (**Dy5**), Ho (**Ho6**), Er (**Er7**), Tm (**Tm8**), Yb (**Yb9**), Lu (**Lu10**) and Y (**Y11**)) polyoxotungstates comprising a single rare earth ion in a rare trigonal prismatic coordination environment, and their characterization in the solid state and in aqueous solutions.

Results and Discussion

Synthesis and crystal structure

Ln*x* polyanions have been prepared in reactions of the phenylphosphonate-stabilized POT, $[P^{V}_4W^{VI}_{24}O_{92}(C_6H_5P^{V}O)_2]^{16-}$ (**P_4W_{24}PhP**) recently reported by us,[24] with the corresponding Ln^{III} salts in a 1:1 molar ratio in 0.5 M $LiCl_{aq}$ medium, acidified with concentrated H_2SO_4 to pH ~ 3.0 (resulting in a weak buffer medium) at 70 °C for 3 days and crystallized as the hydrated potassium or mixed potassium/lithium salts $K_xLn_yH_{12-x-y}[Na\subset\{Ln^{III}(H_2O)\}\{WO(H_2O)\}P_4W_{26}O_{98}]\cdot nH_2O\cdot mLiCl$ ($x = 8.5–11$; $y = 0–2$; $n = 24–34$; $m = 0–1.5$). We note that without acidification of the aqueous LiCl solution the reaction mixture also results in a pH around 3.0 and polyanions **Sm1** to **Y11** are formed; however, in this case some additional Ln^{III} ions act as countercations for the **Ln*x*** POMs. A weak buffer medium circumvents this problem. We hypothesize that this allows to minimize local pH fluctuations during the reaction and hence decreases a decomposition rate of the POT precursor, thus preventing a presence of significant excess of Ln^{III} ions. Interestingly, all **Ln*x*** polyoxoanions incorporate a Na^+ ion in their central cavity, although no Na^+ source was employed. This indicates that either Na^+ plays a crucial role in **Ln*x*** self-assembly or that the inner cavity of $[\{Ln^{III}(H_2O)\}\{WO(H_2O)\}P_4W_{26}O_{98}]^{13-}$ is perfectly structured for the extraction of Na^+ ions from aqueous solutions. The most probable source of Na^+ cations are NaCl impurities present in LiCl.

Importantly, using a similar synthetic approach, namely reactions of **P_4W_{24}PhP** with 3d heterometals, we were also able to isolate Mn^{II} and Cu^{II} derivatives of the same $\{P_4W_{27}\}$ POM archetype as found in **Ln*x***, $[Na\subset\{Mn^{II}(H_2O)\}\{WO(H_2O)\}P_4W_{26}O_{98}]^{13-}$ and $[K\subset\{Cu^{II}(H_2O)\}\{W(OH)(H_2O)\}P_4W_{27}O_{99}]^{14-}$, although the reactions for these derivatives were performed in a sodium acetate buffer medium with higher pH, 4.8).[25] This suggests that **P_4W_{24}PhP** represents a convenient precursor for the species of the $\{MP_4W_{27}\}$ structural type, which until now could not be prepared by any other method. Thus, reactions of well-known $[H_2P_2W_{12}O_{48}]^{12-}$ ($\{P_2W_{12}\}$)[26] and $[H_2P_4W_{24}O_{94}]^{22-}$ ($\{P_4W_{24}\}$)[27] POMs with Ln^{III} ions at similar conditions did not result in **Ln*x*** polyanions. Instead, serious solubility problems and formation of large quantities of barely soluble or even insoluble precipitates were observed in these cases under otherwise identical or similar conditions, and no crystalline products could be isolated. Moreover, no Ln^{III} complexes of $\{P_4W_{24}\}$ and $\{P_2W_{12}\}$ are known.

Single-crystal X-ray diffraction reveals that all eleven compounds of this series crystallize in the monoclinic space group *C*2/*c* (Tables S1–S4 in Supporting Information). Deposition Numbers 2070893 (for K-Sm1), 2070894 (for K-Eu2), 2070895 (for K-Gd3), 2070896 (for KL-Tb4), 2070897 (for K-Dy5), 2070898 (for KL-Ho6), 2070899 (for K-Er7), 2070900 (for K-Tm8), 2070901 (for KL-Yb9), 2071038 (for K-Lu10) and 2071039 (for K-Y11) contain the supplementary crystallographic data for this paper. These data are provided free of charge by the joint Cambridge Crystallographic Data Centre and Fachinformationszentrum Karlsruhe Access Structures service. The compounds are virtually isostructural, differing only in positions and/or site occupancy factors of some countercations and crystal water molecules. The **Ln*x*** clusters contain a $[P_4W_{27}O_{99}(H_2O)]^{16-}$ ($\{P_4W_{27}\}$) POM matrix that fully encloses a single Ln^{III} (or Y^{III}) ion and incorporates a Na^+ cation in its central cavity (Figure 1). Formation of **Ln*x*** from **P_4W_{24}PhP** requires dissociation of phenylphosphonate groups from the precursor and slight rearrangement of its POM skeleton. Thus, in $\{P_4W_{27}\}$ the $\{P_4W_{24}\}$ moiety present in the precursor, formally a V-shaped dimer of two identical $\{P_2W_{12}\}$ units corner-sharing four O atoms, is completed by two peripherally coordinated W^{VI}_p ions, each of which binds to the open end of the $\{P_2W_{12}\}$ building block, and a central W^{VI}_c ion closing off the central cavity of the $\{P_4W_{26}\}$ entity (Figure S2).

All W centers in **Ln*x*** assume the octahedral coordination geometry typical for POTs. Each W_p center coordinates an O atom of a neighboring tetrahedral PO_4 group, one O atom from each of the two terminal W sites of $\{P_2W_{12}\}$, and three oxo atoms, one of which is coordinated to the W_c site and the second one to the Ln^{III} ion. The central W_c ion coordinates to an O atom from both W_p centers, an O atom from the $\{PW_4\}$ belt of the each $\{P_2W_{12}\}$ unit, a μ_2-O binding it to the Ln^{III} ion as well as an exo-oriented terminal aqua ligand (Figures 1 and S2–S3).

The Ln^{III} ions exhibit an unusually low coordination number of six and adopt a nearly C_{2h}-symmetric trigonal prismatic coordination geometry, with isosceles trigonal faces (O···O: 2× 2.69/4.45 Å) and shortest inter-triangle O···O distances of 2.82/2.87/2.97 Å. In this regard, the structure of **Ln*x*** polyanions is very similar to that of the $\{MnP_4W_{27}\}$ POM that we recently reported.[25] One of the faces of the O_6 prism is defined by two O atoms of the peripheral W^{VI} centers (one from each W^{VI} ion) and a μ_2-O connecting it to W_c. The second trigonal face of the O_6 prism is formed by two oxygens of the $\{PW_4\}$ belts of the $\{P_2W_{12}\}$ units located on the opposite sides with respect to oxygens coordinated to W_c, and a H_2O ligand. Alternatively, the Ln coordination environment can be considered as pseudo-bicapped (above the rectangular faces) trigonal prism with two very long Ln···O contacts (2.698(9)–2.897(9) Å) to the O atoms of the $\{PO_4\}$ groups in $\{P_2W_{12}\}$ subunits (see Figure S3; the corresponding bond lengths for all **Ln*x*** are shown in Table S5).

Trigonal prismatic coordination of Ln^{III} ions is not unprecedented,[28] and has also some examples in Ln-POMs chemistry.[19a–c] In a series of dinuclear Ln-POMs with the general formulae $[\{Ln^a(\mu_2\text{-}OH)_2Ln^b\}(\gamma\text{-}SiW_{10}O_{36})_2]^{12-}$ (Ln^a = Gd, Dy; Ln^b =

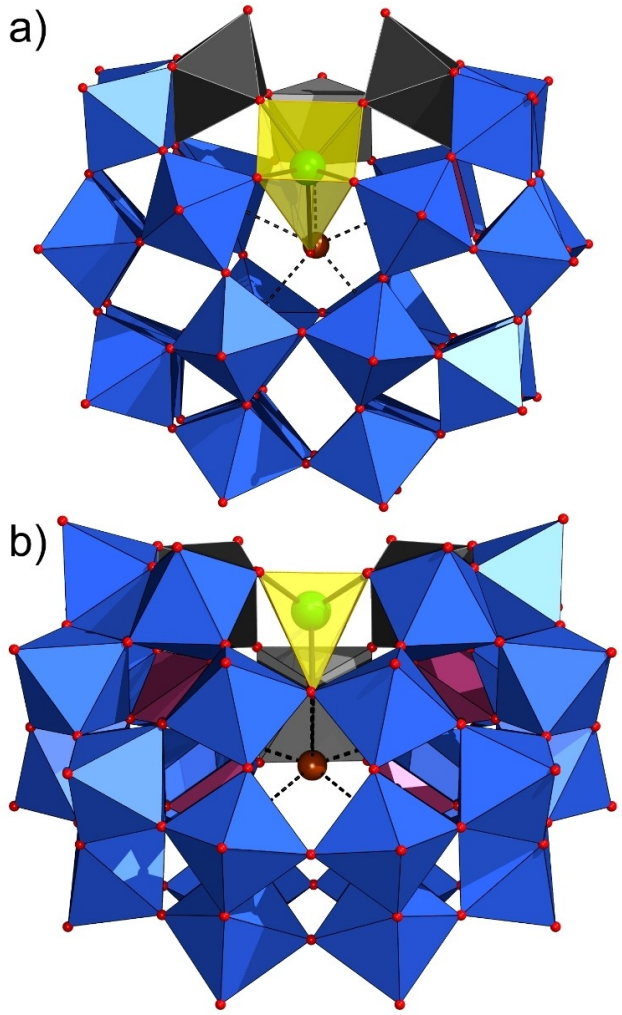

Figure 1. a) Polyhedral representation of the **Lnx** polyanions, with the V-shaped $\{P_2W_{12}\}_2$ substructure shown as blue WO_6 octahedra and purple PO_4 tetrahedra. The upper ends of the $\{P_2W_{12}\}$ units are augmented by two additional edge-sharing WO_6 groups (W_p, dark gray) and a central, corner-sharing WO_6 bridge (W_c, light gray). The Ln site is shown as green sphere and its trigonal prismatic coordination environment is highlighted in transparent yellow (O: small red spheres, Na^+ in central cavity: brown sphere, with shortest Na–O contacts shown as dashed lines). b) The rotated structure, seen perpendicular to the isosceles trigonal face of the LnO_6 coordination polyhedron and emphasizing the C_s symmetry of the polyanion.

Dy, Eu, Yb, Lu)[19a,b] and a giant 3*d*–4*f* nanocluster $[\{(GeW_9O_{34})_2Dy^{III}_3(\mu\text{-}OH)_3(H_2O)\}_6\{Co^{II}_2Dy^{III}_3(\mu_3\text{-}OH)_6(OH_2)_6\}_4]^{56-}$,[19c] reported in the last decade, all (for $\{Ln_2\}$) or some (for $\{Dy_{30}Co_8\}$) Ln^{III} centers reside in (distorted) trigonal prismatic environments. In addition, it was also suggested that some Ce^{IV} ions in $[(H_2O)_n(CeO)_3(PW_9O_{34})_2]^{12-}$ species could lack a terminal aqua ligand, leading to a trigonal prismatic coordination environment.[29] Nevertheless, six-coordinate Ln^{III} complexes remain extremely rare due to high ionic radii of the rare earth metal ions, and most of them display SMM behavior.[28,30] The novel $\{P_4W_{27}\}$ POM archetype appeared to be an ideal scaffold for stabilization of a distorted trigonal prismatic coordination geometry for a wide range of lanthanides and to our knowledge **Lnx** are the first examples of Ln-POMs comprising only a single Ln^{III} ion in such environment.

Curiously, despite apparent structural analogies between the central cavities of $\{LnP_4W_{27}\}$ and $[NaP_5W_{30}O_{110}]^{14-}$,[31] defined by a $\{W_5O_5\}$ and a $\{LnW_4O_5\}$ ring in the former and by two $\{W_5O_5\}$ rings in the latter (Figure S4), their behavior towards Ln^{III} ions differs entirely. Thus, in well-known $[LnP_5W_{30}O_{110}]^{12-}$ complexes Ln^{III} ions are incorporated in the center of the POM structure coordinating 10 O atoms of the $\{W_5O_5\}$ belts plus a terminal H_2O group.[2,6] In our case the Ln^{III} centers showed no tendency to occupy this central position, although we performed numerous attempts varying reaction temperature, medium and time as well as Ln^{III} to $\mathbf{P_4W_{24}PhP}$ ratio in order to prepare such species. Also an attempt to use $\{[Co(H_2O)_4]_2[\{(H_2O)_4Co\}P_4W_{24}O_{92}(C_6H_5PO)_2]\}_n^{10n-}$ ($\{CoP_4W_{24}(PhP)_2\}$)[24] as precursor resulted exclusively in **Lnx** species. In **Lnx** five O atoms of the central $\{W_5O_5\}$ ring are linked to the inner Na^+ ions, additionally binding a terminal aqua ligand on the Ln^{III} center (Figures 1, S4).

In the crystalline lattice, the polyanions **Lnx** are arranged in a 3D framework via a network of ionic bonds with K^+ countercations as well as hydrogen bonds between O sites of the POT skeleton and co-crystallized water molecules. Interestingly, two terminal aqua ligands in **Lnx** also participate in hydrogen bonding. One of them, coordinated to the Ln^{III} center, is encapsulated in the inner cavity of $\{LnP_4W_{27}\}$ (Figure 1) and does not contribute to any intermolecular interactions. However, it forms strong intramolecular hydrogen bonds with four neighboring O atoms of the phosphate groups with O···O distances from 2.50 to 2.75 Å as well as weak hydrogen bonds to the O atoms of the $\{LnW_4O_5\}$ ring (O···O: 2.89–3.32 Å; see Figure S5). At the same time, the terminal aqua ligand on W_c forms a weak hydrogen bond to the O atom of upper $\{PW_6\}$ "belt" of a neighboring polyanion (O6T, Figure S5; O···O: 2.90–3.10 Å) directed approx. along the crystallographic *c* axis (Figures S6, S7). The number of hydrogen bonds of this type formed between each neighboring **Lnx** polyanions depends on the mutual orientation of their Ln^{III} and W_c centers and can vary from 0 (two polyanions facing each other by their Ln^{III} sides) to 1 (the Ln^{III} and W_c sides of the neighboring polyanions alternate) and 2 (two **Lnx** polyanions facing each other by their W_c sides).

Solution studies

^{31}P NMR and UV-Vis spectroscopy

Room-temperature ^{31}P NMR measurements were initially performed on the diamagnetic **K-Y11** derivative dissolved in 0.5 M LiCl aqueous solution acidified to pH ~3.0 with conc. H_2SO_4. The obtained spectrum (Figure 2) exhibits two singlets at −11.28 and −11.57 ppm in an approximate 1:1 integral ratio, which corresponds very well to the presence of two types of symmetrically inequivalent P centers in **Y11**.

The signals of **Y11** are significantly shifted upfield in comparison with singlets at –8.85 and −9.0 ppm observed for

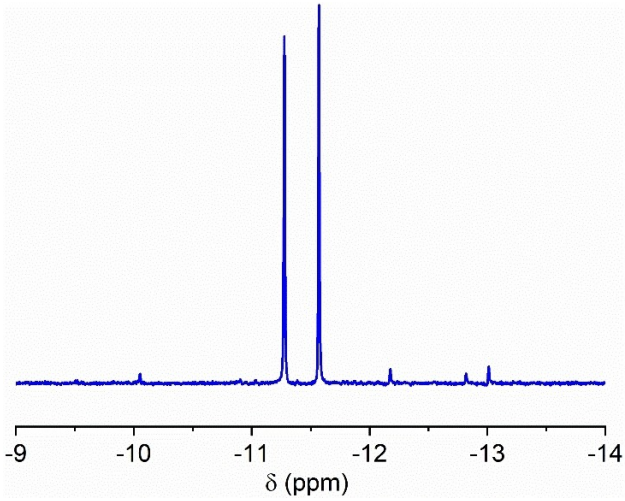

Figure 2. Room-temperature ^{31}P NMR spectrum of **K-Y11** dissolved in 0.5 M LiCl acidified to pH 3.0 with conc. H_2SO_4. The spectra acquired immediately after dissolution of **K-Y11** and after 48 h are identical.

the $\{P_4W_{24}\}$ skeleton in **P_4W_{24}PhP** in H_2O/D_2O,[24] since the P atoms of both structural types in **Y11** are much better shielded from the external magnetic field due to binding of additional W^{VI}, Y^{III} and Na^+ centers in the inner cavity of the polyoxophosphotungstate.

The ^{31}P NMR spectrum recorded on a freshly prepared solution of **K-Y11** is identical to spectra measured after 24 h and after 48 h, indicating high stability of **Y11** in this aqueous medium.

We were also able to record room-temperature ^{31}P NMR spectra for the other derivatives (Figures S21–S30). Most of them also exhibit two signals with relative intensities close to 1:1, one of which is significantly (or in case of **Tb4**, **Dy5**, **Ho6** extremely) broadened. This broadened signal is directly attributed to the P^V centers closest to the magnetic Ln^{III} ion.

For **Gd3** only one broad signal could be observed, while the second one seems to be not visible due to the influence of the $S=7/2$ Gd^{III} center (Figure S23).

In comparison to the spectrum of **K-Y11** solution, the signals in the spectra for the other **Ln*x*** derivatives are significantly shifted upfield or downfield, depending on Ln^{III} ions. The exact chemical shifts values for all **Ln*x*** derivatives are shown in Table S7.

UV-Vis spectra and their evolution over 24 h (see Supporting Information) further support the integrity of the **Ln*x*** polyanions in aqueous solutions.

Cyclic voltammetry

Room-temperature cyclic voltammograms (CVs) for representative polyanions of this series, that is, **Eu2**, **Gd3**, **Tb4** and **Y11**, were recorded on 1 mM solutions of their hydrated salts in 2 M Li_2SO_4/H_2SO_4 buffer (pH ~ 3.0). All polyanions exhibit similar electrochemical properties and for all of them five (quasi-) reversible redox process could be observed before solvent discharge (from −0.25 to −1.0 V; see Figures 3 and S33). The exact potential values for every wave in each case are provided in Table 1. All the redox couples should be attributed to the reduction of the W^{VI} centers in **Ln*x*** ($x=2$, 3, 4 and 11) to W^V ions and their successive re-oxidation upon the increase of the potential. At that, the redox processes for **Eu2** and **Tb4** are observed at slightly more negative potentials in comparison to CV patterns of **Gd3** and **Y11** (Figure S33). No separate redox wave attributed to the reduction of Eu^{III} (in **Eu2**) and Gd^{III} (in **Gd3**) could be distinguished as the redox curves for these derivatives are very similar to those of **Tb4** and **Y11**. The peak currents for all the waves are proportional to the scan rates (Figures S35, S36 and Table S9) indicating the diffusion-controlled electrode reactions.

pH-dependent measurements on solutions of **KN-Gd3** showed that upon an increase of pH from 2.5 to 3.0 (2 M Li_2SO_4/H_2SO_4 buffers) and then further to pH 4.8 (0.5 M NaOAc buffer) all redox waves are shifted towards more negative potentials (Figure S34, Table S8). This reflects that the reduction of W^{VI} in these polyanions is coupled with proton transfer as is very common for POTs.[32] The cyclic voltammogram recorded at pH 4.0 in non-buffered 2 M Li_2SO_4/H_2SO_4 medium generally follows the same trend, however only three redox couples, two of which are not very well separated from each other, could be observed in this medium before solvent discharge (Figure S34).

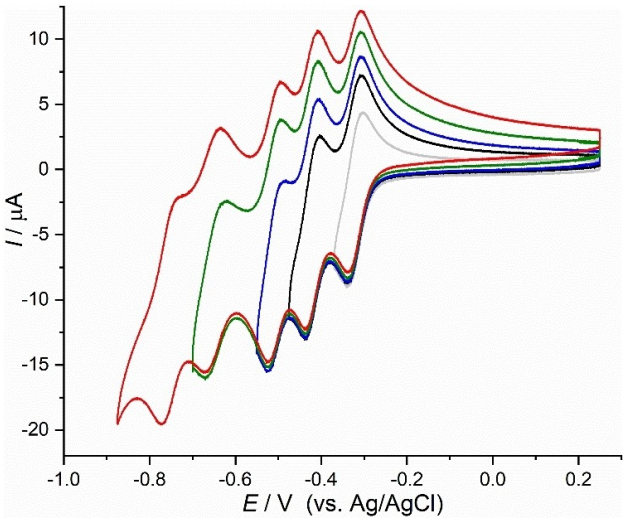

Figure 3. Room-temperature cyclic voltammograms of a 1 mM solution of **KL-Eu2** in 2 M Li_2SO_4/H_2SO_4 buffer (pH ~ 3.0) with different negative potential limits (−0.37 V, −0.475 V, −0.55 V, −0.70 V, and −0.875 V) at a scan rate of 20 mV/s vs. Ag/AgCl reference electrode.

Table 1. $E_{1/2}$ values of redox couples observed in CV for **KL-Eu2**, **K-Gd3**, **KL-Tb4** and **K-Y11** in 2 M Li_2SO_4/H_2SO_4 medium (pH 3.0)

Compound	$E_{1/2}^{I}$ [V]	$E_{1/2}^{II}$ [V]	$E_{1/2}^{III}$ [V]	$E_{1/2}^{IV}$ [V]	$E_{1/2}^{V}$ [V]
KL-Eu2	−0.32	−0.42	−0.51	−0.65	−0.75
K-Gd3	−0.30	−0.40	−0.50	−0.66	−0.78
KL-Tb4	−0.32	−0.42	−0.51	−0.65	−0.75
K-Y11	−0.30	−0.40	−0.50	−0.66	−0.79

A comparison of the CV curves obtained for **Gd3** and previously reported {MnP_4W_{27}} and {CuP_4W_{27}} derivatives[25] in 0.5 M NaOAc buffer (pH 4.8), see Figure S37, clarifies several aspects. Firstly, the first redox couple presumably attributed to the W^{VI} centers directly bound to the heterometal ion[25] appears at nearly the same potential of −0.405 V for the Mn^{II} and Gd^{III} derivatives, which both comprise the heterometal in trigonal prismatic coordination, and at a significantly more positive potential for the Cu^{II}-based species (−0.305 V). The latter could be explained by a release of Cu^{II} ions from the POM due to its reduction to Cu^0 state at −0.18 V. Secondly, all the other redox couples in the CV graph of **Gd3** are shifted to more negative potentials in comparison to the CV curves of the transition metal derivatives, which suggests a higher redox stability for the Ln-POMs. At that, the two waves appearing at most negative potentials (−0.77 V and −0.88 V for **Gd3**) are shifted less than the first three waves. This confirms our previous proposition that these waves reflect redox activity of those W^{VI} centers that are rather distant from the heterometal ion in the POM structure. The redox couple appearing at −0.535 V in the cyclic voltammogram of the Mn^{II} derivative is split into two processes for both Gd^{III}- and Cu^{II}-based polyanions.

Magnetic studies

The static magnetic susceptibility data of the paramagnetic **Ln*x*** compounds are shown in Figure 4. At 290 K and 0.1 T, the $\chi_m T$ values of the compounds are all within the expected range of the respective single Ln^{III} center (Figure 4a):[33] 0.34 (**K-Sm1**, expected: ~0.32), 1.47 (**KL-Eu2**, ca. 1.5), 7.82 (**K-Gd3**, 7.6–7.9), 11.82 (**KL-Tb4**, 11.8–12.0), 13.57 (**K-Dy5**, 13.0–14.1), 13.53 (**K-Ho6**, 13.3–13.8), 11.14 (**K-Er7**, 11.0–11.3), 7.02 (**K-Tm8**, ~7.1) and 2.42 (**KL-Yb9**, ~2.5) $cm^3\,K\,mol^{-1}$. The $\chi_m T$ versus T curves are characterized by shapes typical for each lanthanide center: While $\chi_m T$ for the approximately isotropic Gd^{III} center in **K-Gd3** with a well-isolated ground term remains essentially constant at all temperatures, the $\chi_m T$ versus T curves of the other compounds show temperature-dependent behaviors. At 2.0 K, the $\chi_m T$ values reach 0.04 (**K-Sm1**), 0.02 (**KL-Eu2**), 7.62 (**K-Gd3**), 10.26 (**KL-Tb4**), 11.15 (**K-Dy5**), 7.28 (**K-Ho6**), 8.22 (**K-Er7**), 1.65 (**K-Tm8**) and 1.05 $cm^3\,K\,mol^{-1}$ (**KL-Yb9**). In most cases, the temperature-dependent behavior of the anisotropic Ln^{III} centers is due to the thermal depopulation of the sufficiently energetically isolated, but split $2J+1$ energy states of the respective ground term, which can be characterized in terms of (a mixture of) the quantum numbers m_J. Exceptions are **K-Sm1** and **KL-Eu2**, as their ground terms are close to excited terms, which can also significantly mix into the ground state. In addition, the Zeeman effect may cause weak drop-offs in the curves at the lowest temperatures (< 3–4 K).

In Figure 4b, the molar magnetization M_m as a function of the applied magnetic field B is shown at 2.0 K. As expected for paramagnetic centers, M_m extrapolates to 0 $N_A\,\mu_B$ at 0 T. At fields lower than 1 T, M_m grows steeper than at larger fields. In case of **K-Gd3**, M_m almost saturates (7.0 $N_A\,\mu_B$) with a value of 6.9 $N_A\,\mu_B$ at 5.0 T. For all other compounds, roughly half (±1 $N_A\,\mu_B$) of the saturation values ($g_J\,J\,N_A\,\mu_B$) are found: 0.2 (**K-Sm1**), 0.1 (**KL-Eu2**), 4.9 (**KL-Tb4**), 5.6 (**K-Dy5**), 6.0 (**K-Ho6**), 4.6 (**K-Er7**), 3.1 (**K-Tm8**) and 1.7 $N_A\,\mu_B$ (**KL-Yb9**), in line with measurements of randomly oriented crystallites (powder samples) of significantly anisotropic centers, that is, the observed net magnetizations represent mean values over all magnetic axes.

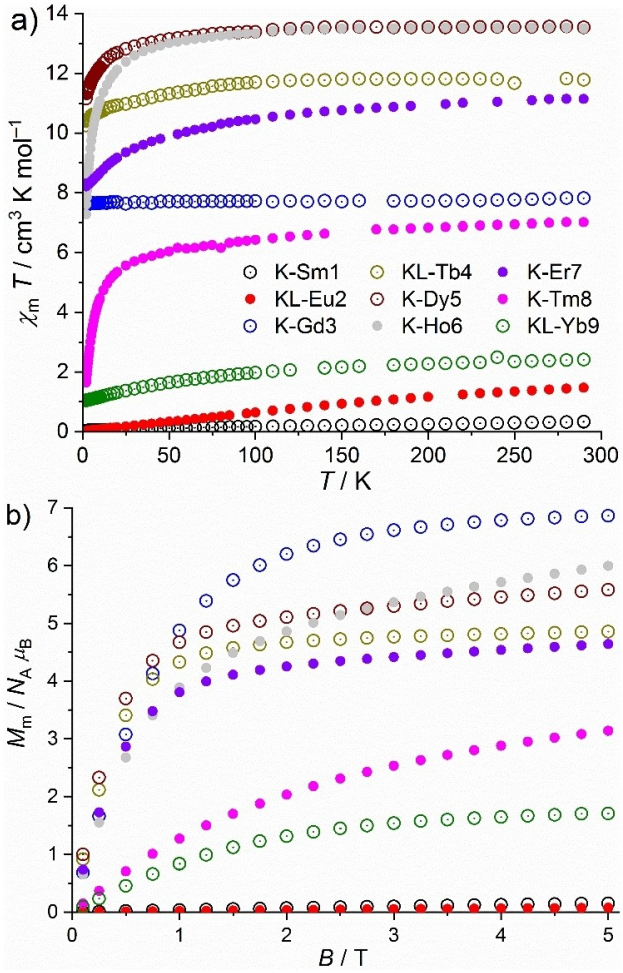

Figure 4. Properties in static magnetic fields (experimental data): a) Temperature dependence of $\chi_m T$ at 0.1 T, and b) molar magnetization M_m vs. applied magnetic field B at 2.0 K.

Ac magnetic susceptibility data in static magnetic bias fields (0 to 1000 Oe) revealed that most of the compounds do not show relevant out-of-phase signals, which could be due to the relatively low ligand field symmetry (approx. C_{2v}) and the corresponding pronounced mixing of various $|m_j>$ contributions into the multiplets.

Only **K-Er7** shows (weak) analyzable signals at zero static bias field (Figure S41). While the signals of **K-Dy5** (Figures 5, S38) and **KL-Yb9** (Figures S42, S43) are optimized for fitting at 1000 Oe and 300 Oe, the weak signals of **K-Ho6** barely change in the probed static field range, and are not suitable for fitting (Figures S39, S40).

Overall, the most pronounced out-of-phase susceptibility component can be observed for **K-Dy5**. In zero static bias field,

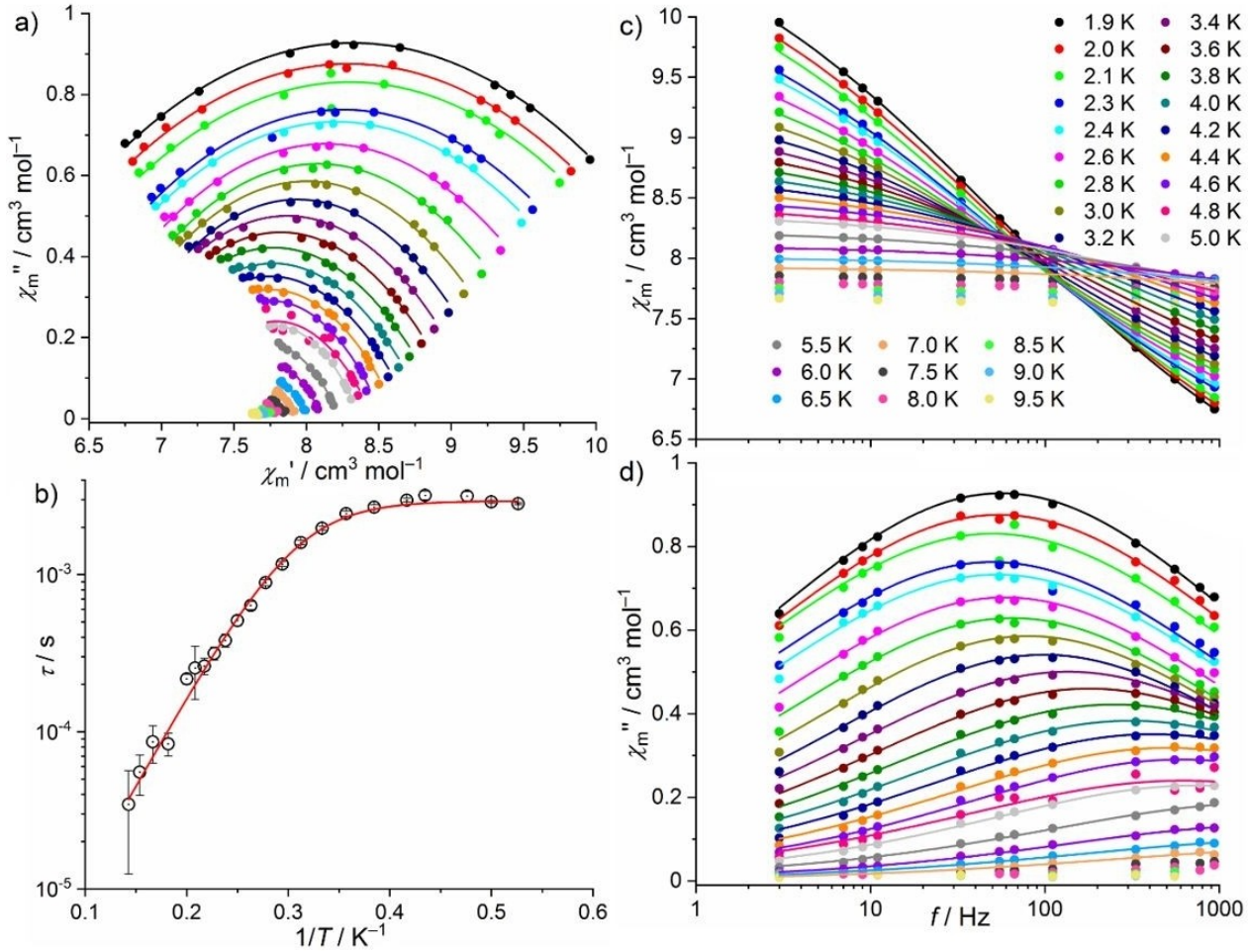

Figure 5. Ac susceptibility measurements of **K-Dy5** in a static magnetic bias field of 1000 Oe: a) Cole-Cole plot of out-of-phase χ_m'' vs. in-phase magnetic susceptibility χ_m', b) relaxation times τ vs. inverse temperature 1/T, c) χ_m' vs. applied frequency f, and d) χ_m'' vs. f (lines: least-squares fits, symbols: data).

weak signals are detected for this sample (see Figure S38) that can be enhanced to a level sufficient for fitting purposes by application of a 1000 Oe bias field (Figure 5). We simultaneously fit the corresponding χ_m' versus f and χ_m'' versus f curves at each temperature using a generalized Debye expression.[34] The results in terms of the relaxation times τ are shown in Figure 5b. Since we find the distribution parameter of these relaxation times to be $\alpha = 0.57 \pm 0.03$, we consider multiple relaxation pathways in the subsequent fit of τ versus 1/T data. The best results are achieved considering an Orbach slow relaxation process and quantum tunneling of magnetization described by the equation $\tau^{-1} = \tau_0^{-1} \exp(-U_{eff}/(k_B T)) + B$. The least-squares fit yields the attempt time $\tau_0 = (8.6 \pm 2.2) \times 10^{-7}$ s, the effective barrier $U_{eff} = (18.4 \pm 0.7)\,cm^{-1}$, and the constant $B = (340 \pm 6)\,s^{-1}$. Since vibrational modes of the ligands generally can influence the slow relaxation behavior, for example through phonon coupling, we explored this effect on the lanthanide ions in the **Ln*x*** polyanions. In their $LnO^{water}O_5^{POT}$ environment, the single H_2O ligand can be replaced by D_2O, and we tentatively assess this effect via deuteration of **K-Dy5**. While a full discussion of the magnetism of deuterated **K-Dy5** (=**K-Dy5-d**) is given in the Supporting Information, we observe a noticable change of the optimal static magnetic bias field (yielding maximum out-of-phase ac susceptibility components) and the associated relaxation parameters: For **K-Dy5-d**, with a bias field of only 500 Oe (vs. 1000 Oe for **K-Dy5**), we find $\tau_0 = (4.5 \pm 0.9) \times 10^{-7}$ s, the effective barrier $U_{eff} = (21.9 \pm 0.7)\,cm^{-1}$, and the constant $B = (985 \pm 10)\,s^{-1}$.

Fitting the signals of **K-Er7** at zero static bias field (see Figure S41) using the generalized Debye expression yields the relaxation times shown in the same figure. Their distribution parameter $\alpha = 0.35 \pm 0.05$ hints at multiple relaxation pathways. The best result is achieved by consideration of an Orbach slow relaxation process and quantum tunneling of magnetization, that is, considering the equation $\tau^{-1} = \tau_0^{-1} \exp(-U_{eff}/(k_B T)) + B$. The least-squares fit yields the attempt time $\tau_0 = (0.7 \pm 6.6) \times 10^{-10}$ s, the effective barrier $U_{eff} = (59 \pm 34)\ cm^{-1}$, and the constant $B = (3427 \pm 94)\ s^{-1}$. We note that the generally weak signals at the maxima of the χ_m'' versus f curves are rather noisy, which results in the slightly scattered data in the τ versus 1/T plot (particularly in the range 0.2–0.3 K^{-1}), and leads in turn to relatively large error margins of the fit parameters. The

analysis of **KL-Yb9** at 300 Oe static bias field (Figure S43) in terms of the generalized Debye expression yields the τ versus $1/T$ plot with $\alpha = 0.07 \pm 0.03$ shown in the same figure. Since α is close to zero, and the curve can be interpreted as linear in this representation within the statistical error margins of the Debye fit, we here consider only a single slow relaxation process (an Orbach process), that is, $\tau = \tau_0 \exp(U_{eff}/(k_B T))$. The corresponding least-squares fit yields the attempt time $\tau_0 = (1.3 \pm 0.3) \times 10^{-5}$ s and the effective barrier $U_{eff} = (3.3 \pm 0.3)$ cm^{-1}. In summary, slow relaxation signals of sufficient magnitude are observed for the Dy^{III} Er^{III} and Yb^{III} derivatives, however, only below 8 K, and the application of a static magnetic bias field is mandatory for quantitative interpretation, with the exception of **K-Er7**. The determined fit parameters are in the typical ranges found for such lanthanides.[35]

Conclusions

Coordination of lanthanide(III) or yttrium(III) ions to the seminal, highly lacunary $\{P_2W_{12}\}$ Wells-Dawson-type building block becomes possible when the recently reported phenylphosphonate-functionalized $\{P_2W_{12}\}$ dimer **P_4W_{24}PhP** is employed. Reactions in weak buffer media result in a rearrangement of the POT framework towards a C_s-symmetric $\{P_4W_{27}\}$ structure, which can be considered as a partially reconstructed C_5-symmetric Preyssler-type cluster, and integration of both a single rare earth heterometal ion and a Na^+ cation into specific binding pockets. The solution-stable products $[Na\subset\{Ln^{III}(H_2O)\}\{WO(H_2O)\}P_4W_{26}O_{98}]^{12-}$ (Ln = Sm, Eu, Gd, Tb, Dy, Ho, Er, Tm, Yb, Lu and Y) represent the first examples of POMs comprising a discrete, trigonal-prismatically coordinated lanthanide(III) or yttrium(III) ion. Electrochemical studies revealed redox behavior associated with five consecutive (quasi-)reversible redox couples attributed to proton-coupled $W^{VI} \leftrightarrow W^{V}$ transformations. The Dy, Ho, Er, and Yb derivatives display weak out-of-phase components in their ac magnetic susceptibility. For the Dy derivative, the exchange of the single water ligand with D_2O significantly affects the out-of-phase components and the parameters of the relevant relaxation processes.

Acknowledgements

We gratefully acknowledge financial support by Forschungszentrum Jülich, EU ERC Starting Grant 308051–MOLSPINTRON and German Science Foundation (Grant DFG-IZ-60/3-1). T.I. appreciates The Punjab Educational Endowment Fund (PEEF) for a doctoral fellowship (CMMS scholarship program). We thank Brigitte Jansen for TGA and Christina Houben for SQUID measurements. Open access funding enabled and organized by Projekt DEAL.

Conflict of Interest

The authors declare no conflict of interest.

Keywords: electrochemistry · lanthanides · polyoxometalates · six-coordinate · SQUID

[1] a) Q. Luo, R. C. Howell, L. C. Francesconi, in *Polyoxometalate Chemistry for Nano-Composite Design. Nanostructure Science and Technology* (Eds.: T. Yamase, M. T. Pope), Springer, Boston, **2002**, p. 73–81; b) B. S. Bassil, U. Kortz, *Z. Anorg. Allg. Chem.* **2010**, *636*, 2222–2231; c) J.-W. Zhao, Y.-Z. Li, L.-J. Chen, G.-Y. Yang, *Chem. Commun.* **2016**, *52*, 4418–4445; d) C. Boskovic, *Acc. Chem. Res.* **2017**, *50*, 2205–2214.
[2] *See for example*: I. Creaser, M. C. Heckel, R. J. Neitz, M. T. Pope, *Inorg. Chem.* **1993**, 32, 1573–1578.
[3] G. A. Barbieri, *Rend. Mat. Acc. Lincei* **1914**, *23*, 805–812.
[4] R. D. Peacock, T. J. R. Weakley, *J. Chem. Soc. A* **1971**, 1836–1839.
[5] U. Kortz, C. Holzapfel, M. Reicke, *J. Mol. Struct.* **2003**, *656*, 93–100.
[6] *See for example*: a) K.-C. Kim, M. T. Pope, G. J. Gama, M. H. Dickman, *J. Am. Chem. Soc.* **1999**, *121*, 11164–11170; b) S. Cardona-Serra, J. M. Clemente-Juan, E. Coronado, A. Gaita-Ariño, A. Camón, M. Evangelisti, F. Luis, M. J. Martínez-Pérez, J. Sesé, *J. Am. Chem. Soc.* **2012**, *134*, 14982–14990; c) C. Kato, R. Machida, R. Maruyama, R. Tsunashima, X.-M. Ren, M. Kurmoo, K. Inoue, S. Nishihara, *Angew. Chem. Int. Ed.* **2018**, *57*, 13429–13432; *Angew. Chem.* **2018**, *130*, 13617–13620.
[7] *See for example*: a) V. N. Molchanov, L. P. Kazansky, E. A. Torchenkova, V. I. Simonov, *Kristallografiya* **1979**, *24*, 167–168; b) A. Ostuni, R. E. Bachman, M. T. Pope, *J. Cluster Sci.* **2003**, *14*, 431–446; c) R. Wan, P. Ma, M. Han, D. Zhang, C. Zhang, J. Niu, J. Wang, *Dalton Trans.* **2017**, *46*, 5398–5405; d) J. Iijima, H. Naruke, T. Sanji, *Inorg. Chem.* **2018**, *57*, 13351–13363.
[8] *See for example*: a) M. Sadakane, A. Ostuni, M. T. Pope, *Dalton Trans.* **2002**, 63–67; b) Q. Luo, R. C. Howell, J. Bartis, M. Dankova, W. DeW. Horrocks Jr., A. L. Rheingold, L. C. Francesconi, *Inorg. Chem.* **2002**, *41*, 6112–6117; c) W. Wang, N. V. Izarova, J. van Leusen, P. Kögerler, *Cryst. Growth Des.* **2019**, *19*, 4860–4870.
[9] a) C. Ritchie, E. G. Moore, M. Speldrich, P. Kögerler, C. Boskovic, *Angew. Chem. Int. Ed.* **2010**, *49*, 7702–7705; *Angew. Chem.* **2010**, *122*, 7868–7871; b) C. Ritchie, V. Baslon, E. G. Moore, C. Reber, C. Boskovic, *Inorg. Chem.* **2012**, *51*, 1142–1151.
[10] K. Wassermann, M. H. Dickman, M. T. Pope, *Angew. Chem. Int. Ed.* **1997**, *36*, 1445–1448; *Angew. Chem.* **1997**, *109*, 1513–1516.
[11] B. S. Bassil, M. H. Dickman, I. Römer, B. von der Kammer, U. Kortz, *Angew. Chem. Int. Ed.* **2007**, *46*, 6192–6195; *Angew. Chem.* **2007**, *119*, 6305–6308.
[12] X. Fang, T. M. Anderson, C. Benelli, C. L. Hill, *Chem. Eur. J.* **2005**, 712–718.
[13] P. Ma, R. Wan, Y. Wang, F. Hu, D. Zhang, J. Niu, J. Wang, *Inorg. Chem.* **2016**, *55*, 918–924.
[14] Z. Li, X.-X. Li, T. Yang, Z.-W. Cai, S.-T. Zheng, *Angew. Chem. Int. Ed.* **2017**, *56*, 2664–2669; *Angew. Chem.* **2017**, *129*, 2708–2713.
[15] *See for example*: a) D. N. Woodruff, R. E. P. Winpenny, R. A. Layfield, *Chem. Rev.* **2013**, *113*, 5110–5148; b) H. L. C. Feltham, S. Brooker, *Coord. Chem. Rev.* **2014**, *276*, 1–33; c) O. Cador, B. Le Guennic, F. Pointillart, *Inorg. Chem. Front.* **2019**, *6*, 3398–3417.
[16] M. A. AlDamen, J. M. Clemente-Juan, E. Coronado, C. Martí-Gastaldo, A. Gaita-Ariño, *J. Am. Chem. Soc.* **2008**, *130*, 8874–8875.
[17] *See for example*: a) M. A. AlDamen, S. Cardona-Serra, J. M. Clemente-Juan, E. Coronado, A. Gaita-Ariño, C. Martí-Gastaldo, F. Luis, O. Montero, *Inorg. Chem.* **2009**, *48*, 3467–3479; b) P. Ma, F. Hu, Y. Huo, D. Zhang, C. Zhang, J. Niu, J. Wang, *Cryst. Growth Des.* **2017**, *17*, 1947–1956; c) A. S. Mougharbel, S. Bhattacharya, B. S. Bassil, A. Rubab, J. van Leusen, P. Kögerler, J. Wojciechowski, U. Kortz, *Inorg. Chem.* **2020**, *59*, 4340–4348.
[18] *See for example*: a) J. J. Baldoví, Y. Duan, C. Bustos, S. Cardona-Serra, P. Gouzerh, R. Villanneau, G. Gontard, J. M. Clemente-Juan, A. Gaita-Ariño, C. Giménez-Saiz, A. Proust, E. Coronado, *Dalton Trans.* **2016**, *45*, 16653–16660; b) Z. Jin, J. Bai, T. Wei, F. Li, C. Song, X. Luo, L. Xu, *New J. Chem.* **2017**, *41*, 13490–13494.
[19] *See for example*: a) K. Suzuki, R. Sato, N. Mizuno, *Chem. Sci.* **2013**, *4*, 596–600; b) R. Sato, K. Suzuki, M. Sugawa, N. Mizuno, *Chem. Eur. J.* **2013**, *19*, 12982–12990; c) M. Ibrahim, V. Mereacre, N. Leblanc, W. Wernsdorfer, C. E. Anson, A. K. Powell, *Angew. Chem. Int. Ed.* **2015**, *54*, 15574–15578; *Angew. Chem.* **2015**, *127*, 15795–15799; d) M. J. Giansiracusa, M. Vonci, W. Van den Heuvel, R. W. Gable, B. Moubaraki, K. S. Murray, D. Yu, R. A. Mole, A. Soncini, C. Boskovic, *Inorg. Chem.* **2016**, *55*, 5201–5214; e) Y. Huo, Y.-C. Chen, S.-G. Wu, J.-H. Jia, W.-B. Chen, J.-L. Liu, M.-L. Tong, *Inorg. Chem.* **2018**, *57*, 6773–6777; f) H. Chen, L. Sun, J. Zhang, Z. Xiao, P. Ma, J. Wang, Y. Zhang, J. Niu, *Dalton Trans.* **2020**, *49*, 12458–12465; g) J. Xiong,

Z.-X. Yang, P. Ma, D. Lin, Q. Zheng, Y. Huo, *Inorg. Chem.* **2021**, *60*, 7519–7526.
[20] a) J. J. Baldoví, S. Cardona-Serra, A. Gaita-Ariño, E. Coronado, *Adv. Inorg. Chem.* **2017**, *69*, 213–249; b) A. Gaita-Ariño, F. Luis, S. Hill, E. Coronado, *Nat. Chem.* **2019**, *11*, 301–309; c) E. Coronado, *Nat. Rev. Mat.* **2020**, *5*, 87104 and references therein.
[21] a) J. J. Baldoví, S. Cardona-Serra, J. M. Clemente-Juan, E. Coronado, A. Gaita-Ariño, H. Prima-García, *Chem. Commun.* **2013**, *49*, 8922–8924; b) M. D. Jenkins, Y. Duan, B. Diosdado, J. J. García-Ripoll, A. Gaita-Ariño, C. Giménez-Saiz, P. J. Alonso, E. Coronado, F. Luis, *Phys. Rev. B* **2017**, *95*, 064423 : 1-8.
[22] M. Shiddiq, D. Komijani, Y. Duan, A. Gaita-Ariño, E. Coronado, S. Hill, *Nature* **2016**, *531*, 348–351.
[23] J. J. Baldoví, L. E. Rosaleny, V. Ramachandran, J. Christian, N. S. Dalal, J. M. Clemente-Juan, P. Yang, U. Kortz, A. Gaita-Ariño, E. Coronado, *Inorg. Chem. Front.* **2015**, *2*, 893–897.
[24] X. Yi, N. V. Izarova, P. Kögerler, *Chem. Commun.* **2018**, *54*, 2216–2219.
[25] T. Iftikhar, N. V. Izarova, J. van Leusen, P. Kögerler, *Chem. Eur. J.* **2021**, *27*, 8500–8508.
[26] a) R. Contant, in *Inorganic Synthesis*, *Vol. 27* (Ed: A. P. Ginsberg), John Wiley and Sons, New York, **1990**; p. 104 – 111; b) R. Contant, J. P. Ciabrini, *J. Chem. Res.* **1977**, *222*, 2601–2617.
[27] R. Contant, A. Tézé, *Inorg. Chem.* **1985**, *24*, 4610–4614.
[28] *See for example*: a) K. R. Miehaus, S. G. Minasian, W. W. Lukens Jr, S. A. Kozimor, D. K. Shuh, T. Tyliszczak, J. R. Long, *J. Am. Chem. Soc.* **2014**, *136*, 6056–6068; b) S. Liu, Y. Meng, Y. Zhang, Z. Meng, K. Lang, Z. Zhu, C. Shang, B. Wang, S. Gao, *Inorg. Chem.* **2017**, *56*, 7320–7323; c) T. P. Latendresse, V. Vieru, A. Upadhyay, N. S. Bhuvanesh, L. F. Chibotaru, M. Nippe, *Chem. Sci.* **2020**, *11*, 3936–3951.
[29] W. H. Knoth, P. J. Domaille, R. L. Harlow, *Inorg. Chem.* **1986**, *25*, 1577–1584.
[30] *See for example*: a) J.-L. Liu, K. Yuan, J.-D. Leng, L. Ungur, W. Wernsdorfer, F.-S. Guo, L. F. Chibotaru, M.-L. Tong, *Inorg. Chem.* **2012**, *51*, 8538–8544; b) R. J. Blagg, L. Ungur, F. Tuna, J. Speak, P. Comar, D. Collison, W. Wernsdorfer, E. J. L. McInnes, L. F. Chibotaru, R. E. P. Winpenny, *Nat. Chem.* **2013**, *5*, 673–678; c) M.-X. Yao, Z.-X. Zhu, X.-Y. Lu, X.-W. Deng, S. Jing, *Dalton Trans.* **2016**, *45*, 10689–10695.
[31] M. H. Alizadeh, S. P. Harmalker, Y. Jeannin, J. Martin-Frère, M. T. Pope, *J. Am. Chem. Soc.* **1985**, *107*, 2662–2669.
[32] T. Ueda, *ChemElectroChem* **2018**, *5*, 823–838.
[33] H. Lueken, *Magnetochemie*, Teubner Verlag, Stuttgart, **1999**.
[34] K. S. Cole, R. H. Cole, *J. Chem. Phys.* **1941**, *9*, 341–351.
[35] D. N. Woodruff, R. E. P. Winpenny, R. A. Layfield, *Chem. Rev.* **2013**, *113*, 5110–5148.

Manuscript received: April 25, 2021
Accepted manuscript online: July 14, 2021
Version of record online: August 19, 2021

